



**Thermally Stable Nanometals by Predictive Atomic Scale
Interfacial Energy Reduction**

**by Dr. Kris Darling, Dr. Laszlo Kecskes, Professor Zi-Kui Liu,
Professor Elizabeth Dickey, and Dr. Jing Li**

ARL-TR-5490

March 2011

NOTICES

Disclaimers

The findings in this report are not to be construed as an official Department of the Army position unless so designated by other authorized documents.

Citation of manufacturer's or trade names does not constitute an official endorsement or approval of the use thereof.

Destroy this report when it is no longer needed. Do not return it to the originator.

Army Research Laboratory

Aberdeen Proving Ground, MD 21005-5069

ARL-TR-5490

March 2011

Thermally Stable Nanometals by Predictive Atomic Scale Interfacial Energy Reduction

Dr. Kris Darling and Dr. Laszlo Kecskes
Weapons and Materials Research Directorate, ARL

Professor Zi-Kui Liu, Professor Elizabeth Dickey, and Dr. Jing Li
Dept. of Materials Science & Engineering
The Pennsylvania State University, University Park, PA 16802

REPORT DOCUMENTATION PAGE

Form Approved
OMB No. 0704-0188

Public reporting burden for this collection of information is estimated to average 1 hour per response, including the time for reviewing instructions, searching existing data sources, gathering and maintaining the data needed, and completing and reviewing the collection information. Send comments regarding this burden estimate or any other aspect of this collection of information, including suggestions for reducing the burden, to Department of Defense, Washington Headquarters Services, Directorate for Information Operations and Reports (0704-0188), 1215 Jefferson Davis Highway, Suite 1204, Arlington, VA 22202-4302. Respondents should be aware that notwithstanding any other provision of law, no person shall be subject to any penalty for failing to comply with a collection of information if it does not display a currently valid OMB control number.

PLEASE DO NOT RETURN YOUR FORM TO THE ABOVE ADDRESS.

1. REPORT DATE (DD-MM-YYYY) March 2011		2. REPORT TYPE DRI		3. DATES COVERED (From - To) FY10	
4. TITLE AND SUBTITLE Thermally Stable Nanometals by Predictive Atomic Scale Interfacial Energy Reduction				5a. CONTRACT NUMBER	
				5b. GRANT NUMBER	
				5c. PROGRAM ELEMENT NUMBER	
6. AUTHOR(S) Dr. Kris Darling and Dr. Laszlo Kecskes, Professor Zi-Kui Liu, Professor Elizabeth Dickey, and Dr. Jing Li				5d. PROJECT NUMBER	
				5e. TASK NUMBER	
				5f. WORK UNIT NUMBER	
7. PERFORMING ORGANIZATION NAME(S) AND ADDRESS(ES) U.S. Army Research Laboratory ATTN: RDRL-WMM-F Aberdeen Proving Ground, MD 21005				8. PERFORMING ORGANIZATION REPORT NUMBER ARL-TR-5490	
9. SPONSORING/MONITORING AGENCY NAME(S) AND ADDRESS(ES)				10. SPONSOR/MONITOR'S ACRONYM(S)	
				11. SPONSOR/MONITOR'S REPORT NUMBER(S)	
12. DISTRIBUTION/AVAILABILITY STATEMENT Approved for public release; distribution unlimited.					
13. SUPPLEMENTARY NOTES					
14. ABSTRACT Nanocrystalline iron (Fe) alloys doped with 1 at.% zirconium (Zr), tantalum (Ta), and nickel (Ni), produced through high energy mechanical alloying, were investigated for microstructural stability. The results were consistent with theoretical predictions, indicating a decrease in stability with solute type in the following order: Zr, Ta, and Ni. Preliminary transmission electron microscopy (TEM) investigations of the most stable system, Fe-Zr, revealed the presence of 2.5 at.% Zr within the grain boundaries of the sample, confirming a thermodynamic tendency for stability. More specifically, Zr segregation was found to be inhomogeneously distributed between grain boundaries of nanostructured regions. Such a distribution accounts for and provides a potential mechanism for the appearance of abnormal grain growth at elevated temperatures. Additional compositional profiling uncovered a new FCC phase, within the abnormally grown grains. This phase is coherent with the BCC Fe substrate matrix and has a lattice parameter of 8.5 Å.					
15. SUBJECT TERMS Solute Segregation, Nanocrystalline, Thermodynamic Stability, Abnormal Grain Growth					
16. SECURITY CLASSIFICATION OF:			17. LIMITATION OF ABSTRACT UU	18. NUMBER OF PAGES 28	19a. NAME OF RESPONSIBLE PERSON Kris Darling
a. REPORT Unclassified	b. ABSTRACT Unclassified	c. THIS PAGE Unclassified			19b. TELEPHONE NUMBER (Include area code) (410) 306-0862

Contents

List of Figures	iv
List of Tables	v
1. Objective	1
2. Approach	1
2.1 Production and Initial Characterization of the Nanocrystalline Alloys	2
2.2 Advanced Micro Structural Analysis	2
2.3 Atomistic Modeling.....	3
2.4 Milestones	3
3. Results	3
4. Conclusions	16
5. References	17
6. Transitions	18
List of Symbols, Abbreviations, and Acronyms	19
Distribution List	20

List of Figures

Figure 1. Plot of Fe interfacial energy vs. interfacial solute concentration for various solutes.....	4
Figure 2. Grain size vs. annealing temperature for various Fe alloys.....	5
Figure 3. Optical micrographs for pure Fe after annealing 1 h at the given temperatures. Percent area abnormally grown is indicated, respectively.....	6
Figure 4. Focused ion beam contrast images for pure Fe after annealing at 616 °C.....	6
Figure 5. Optical micrographs for Fe 1 at.% Ni after annealing 1 h at the given temperatures. Percent area abnormally grown is indicated, respectively.....	7
Figure 6. Focused ion beam contrast images for Fe 1 at.% Ni after annealing at 700 °C.....	7
Figure 7. Optical micrographs for Fe 1 at.% Ta and Fe 1 at.% Zr after annealing 1 h at the given temperatures. Percent area abnormally grown is indicated, respectively.....	8
Figure 8. Focused ion beam contrast images for Fe 1 at.% Ta and Fe 1 at.% Zr after annealing 1 h at the given temperatures.....	8
Figure 9. Plot showing the percent area remaining nanocrystalline for the various alloys vs. annealing temperature.....	9
Figure 10. Bright and dark field TEM images of Fe 1 at.% Zr annealed at 900 °C. Images show a single micron-sized grain and a region containing nanocrystalline grains.....	10
Figure 11. High resolution TEM image of Fe 1 at.% Zr annealed at 900 °C giving regions where EDS was performed to quantify Zr solute content in the boundary region.....	11
Figure 12. Corresponding solute profile for figure 11 (Series 1).....	11
Figure 13. High resolution TEM image of Fe 1 at.% Zr annealed at 900 °C giving regions where EDS was performed to quantify Zr solute content in the boundary regions between nanograins.....	12
Figure 14. Corresponding solute profile for figure 13 (GB2).....	12
Figure 15. Bright and dark field TEM images of Fe 1 at.% Zr annealed at 700 °C. Images show elongated grain with a single micron-sized grain and a region containing nanocrystalline grains with an average aspect ratio of 10:1.....	13
Figure 16. High resolution TEM image of Fe 1 at.% Zr annealed at 700 °C giving regions where EDS was performed to quantify Zr solute content in the boundary region.....	13
Figure 17. High resolution TEM images of Fe 1 at.% Zr annealed at 900 °C giving figure 17: Precipitates contained within abnormally grown grain. (a) Precipitates showing average size of 5 nm, (b) a larger precipitate showing coherency, and (c) a Fourier filtered high resolution TEM image using the second phase pattern in (b), showing a superlattice of FCC <110> ($a_0 = 8.5 \text{ \AA}$), which is overlapped on the α -Fe <001> lattice.....	14
Figure 18. High resolution TEM images of Fe 1 at.% Zr annealed at 900 °C giving precipitates contained within abnormally grown grain. EELS spectra (a) and (b) for nanocrystals given in the high resolution TEM image above.....	15

List of Tables

Table 1. Thermodynamic parameters for select solutes in Fe.	4
--	---

INTENTIONALLY LEFT BLANK.

1. Objective

Our objective is to understand the electronic contribution to solute/solvent systems to enable a more robust methodology to predict future alloy systems, which cannot be achieved with existing strategies. Particularly, we intend to use state-of-the-art atomic-level characterization techniques to identify and determine the electronic contributions responsible for reducing and minimizing the interfacial energy of high-temperature nanocrystalline alloys relevant to U.S. Army applications. It is the predictive power of this new model, made possible by knowledge of the electronic structure, which, in turn, will allow for a non-empirical approach to alloy development.

Initially, the transmission electron microscopy (TEM) and analysis aspects of the effort were to be contracted to Oak Ridge National Laboratory. The initial kick off meeting at Oak Ridge took place and contract processing was initiated. Samples were sent such that work could begin once the contract was in place. After a few months of inconsistent communications and the failure to complete the contract initiation forms, a new source was identified. As such, funds were diverted to Prof. Zi-Kui Liu at Pennsylvania State University, and the contract process was restarted. Additionally, because the samples from Oak Ridge could not be recovered, new samples had to be made. Funds were released to Pennsylvania State University on August 27, 2010. The objectives have remained the same and experiments are currently underway.

2. Approach

Interfacial energy reduction has been suggested to be a superior method to prevent grain growth in nanocrystalline materials, as compared to kinetic pinning of grain boundaries by secondary phases. Since grain boundary mobility follows an Arrhenius behavior, all kinetic pinning processes are temperature dependent and temperature limited. Recently, it was reported by Krill et al. (1) that the addition of zirconium (Zr) to palladium (Pd) led to an alloy that retained its nanocrystalline microstructure (<100 nm) up to ~1500 °C, or 95% of its melting temperature. A large interfacial energy reduction of approximately 70% was cited as the reason for the thermal stability. In particular, the release in elastic enthalpy upon Zr solute segregation to the interfacial boundaries was identified as the actual mechanism responsible for the large energy reduction. Additional experimental studies on interfacial energy reduction, via grain boundary segregation of solutes, have been reported, e.g., niobium (Nb)-copper (Cu), ruthenium aluminum (RuAl)-iron (Fe), yttrium (Y)-Fe, titanium oxide (TiO₂)-calcium (Ca), etc. (2–8). However, these experiments have little impact on the interests of the U.S. Army.

Instead, as a first principles demonstration of the solute prediction method, we proposed to develop stable nanocrystalline alloys by the additions of select solutes to Fe, which would exhibit extraordinary thermal stability. Elemental additions to the selected base metals would result in engineering alloys that will exhibit a large interfacial energy reduction as the sole means of thermal stability (excluding kinetic effects). For comparison, further elements were to be added to the base metal(s) to demonstrate that little or no interfacial energy reduction would result if certain selection rules are ignored. Specifically, other parameters such as the electro negativity difference, free surface energies difference, solubility limits, heats of mixing (+/-), and atomic size difference are not taken into consideration. However, in this study, they will be varied. More importantly, the electronic contributions of the solute at the interface, as it pertains to interfacial energy reduction, have largely been ignored. To our knowledge, there are no ongoing experimental efforts that have investigated the effect of electronic contributions to interfacial energy reduction. This is despite the large influence of these contributions on grain boundary attributes. In part, these effects have been ignored because the characterization of electronic structure, due to solutes in grain boundaries at the nanoscale, is an extreme challenge in itself. Specifically, the prediction of the solute atom in any base metal system entails an intricate knowledge of the mechanisms contributing to the total free energy change of the system, including characterization of the bulk/surface impurity sites, analysis of possible relaxation states around the impurity atom, core level binding energy shifts, and partitioned electron density and orbital hybridization.

2.1 Production and Initial Characterization of the Nanocrystalline Alloys

High energy mechanical milling was used to alloy and reduce the microstructure to the nanoscale (<50 nm) regime. Isothermal annealing studies were performed, along with x-ray line broadening measurements and TEM in order to estimate the thermal stability.

2.2 Advanced Micro Structural Analysis

The grain boundary and interfacial structure was analyzed using electron energy loss spectroscopy (EELS). More specifically, energy loss near edge structure (ELNES) analysis, in combination with Z-contrast imaging, is used as the main characterization method in addition to energy dispersive spectroscopy (EDS). Such analysis is an effective way to separate differences in electronic structures at the interface and how it relates to the overall interfacial energy reduction of the specific alloy system. Additionally, such techniques can give information on how much solute resides in the grain boundaries; how the solute is distributed (homogeneously/in homogeneously) among the grain boundaries; and if Zr solute is distributed uniformly, whether the interfacial energy reduction is homogenous.

2.3 Atomistic Modeling

In upcoming work, atomistic models are to be used in combination with density functional theory (DFT) to yield the energy and atomic configurations of the grain boundaries, their associated electron distribution (charge density) site, and momentum resolved density of states and ELNES structures. Modeling and calculations of ELNES structures will be performed for all experimental cases, using supporting EELS data and will be compared to the electronic structures of the grain boundaries, with or without the presence of solute atoms.

2.4 Milestones

The following are the milestones for this effort:

- First Quarter: Fabricate solute-stabilized metal specimens (completed).
 - Second Quarter: Conduct atomic characterization to extract electronic contributions to interfacial energy reduction; interim report (ongoing).
 - Third Quarter: Build a DFT simulation using experimentally derived electronic contributions (to be performed).
 - Fourth Quarter: Match the model to experimental results and use the model to predict new system; final report (to be completed).
-

3. Results

The current model, equation 1, used to estimate the effect of various solutes on decreasing grain boundary energy for a given system, is given below. The model takes into consideration the elastic enthalpy change, ΔE_{el} , and the change in cohesive energy for both the lattice and grain boundary area:

$$\gamma = \gamma_o - \frac{2x_A^*}{\sigma} \left[\sigma \frac{\gamma_A^s - \gamma_{Fe}^s}{6} - \frac{\Delta H_{mix}}{3} \left(17x_A^* + \frac{1}{2} \right) - \Delta E_{el} \right]. \quad (1)$$

γ is the effective grain boundary energy after solute segregation; γ_o is the initial grain boundary energy; x_A^* is the interfacial solute concentration; σ is the molar interfacial area and is equal to $v_B^{2/3} N_{AVG}$, where v_B is the atomic volume and N_{AVG} is the Avogadro number; and ΔH_{mix} is the equimolar ($x_A = x_B$) enthalpy of mixing in the liquid state. Based on equation 1, solutes were selected (table 1). Using these values (7) in equation 1 provides the graph shown in figure 1.

Table 1. Thermodynamic parameters for select solutes in Fe.

Solute	γ_A^s (J/m ²)	ΔE_{el} (kJ/mol)	ΔH_{mix} (kJ/mol)
Cr	2.3	0	-1
Ni	2.45	1	-2
Ta	3.15	61	-15
Zr	2.0	92	-25
Y	1.12	95	-1

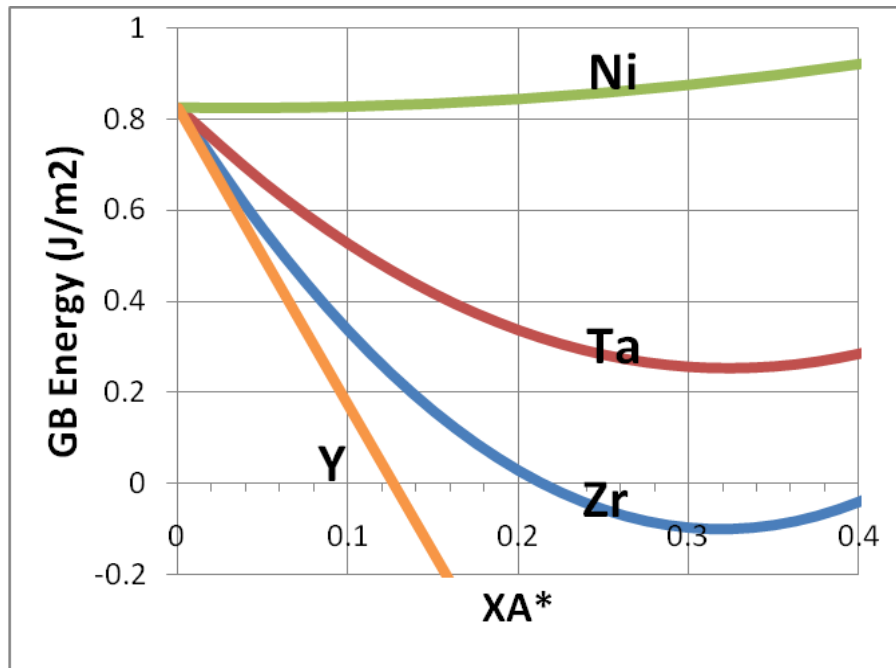


Figure 1. Plot of Fe interfacial energy vs. interfacial solute concentration for various solutes.

Figure 1 depicts the effectiveness of the given solutes for decreasing the grain boundary energy in nanocrystalline Fe and suggests the addition of Ni to Fe does not stabilize the microstructure. However, tantalum (Ta), Zr, and Y appear to have a large effect on reducing the interfacial energy, and hence, stabilizing the microstructure. Y is excluded experimentally, as grain boundary embrittlement would be a concern; this is based on Hondros's correlation (8).

Mechanical alloying was used to create solid solutions of select alloys, those being Fe 1 at.% nickel (Ni), Fe 1 at.% Ta, and Fe 1 at.% Zr. The idea being that upon annealing, solute would either be incorporated into the grain boundaries as they expanded or be interfacially segregated there. Figure 2 gives the x-ray estimated grain size of the given alloys versus annealing temperature. Fe with 1 at.% Ni follows the same grain growth trend as pure Fe, whereas

Fe 1 at.% Ta and Fe 1 at.% Zr show significant reduction in grain growth. These experimental results are in good agreement with the theoretical predictions that were given graphically in figure 1.

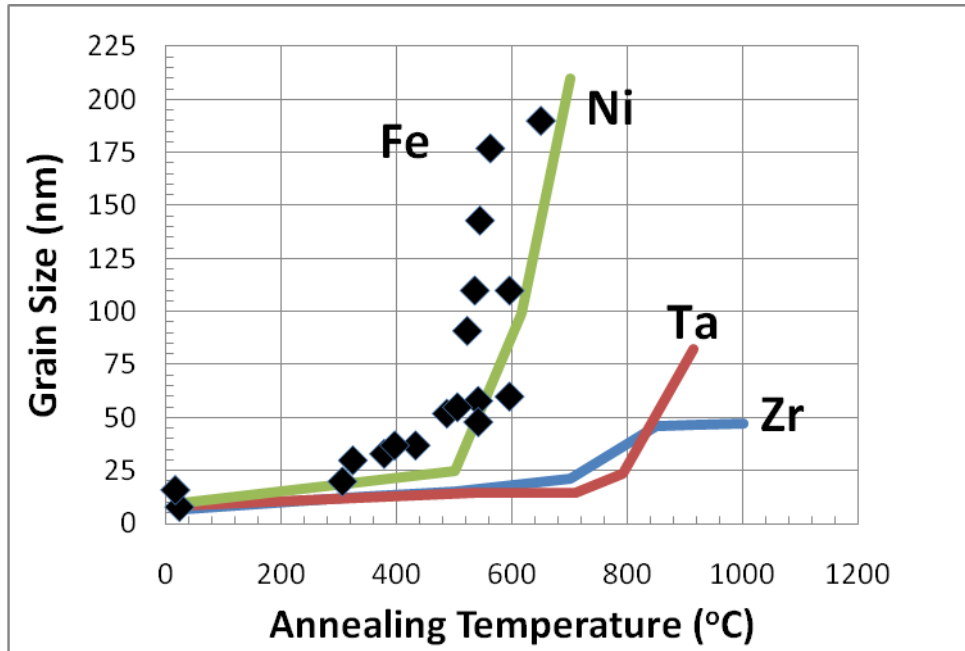


Figure 2. Grain size vs. annealing temperature for various Fe alloys.

To investigate the stability of the alloys further, additional investigations were conducted. Optical images of polished and etched cross sections of the samples revealed a bimodal grain size distribution in the form of dark gray regions and white regions. Micrometer-scale grains could be distinguished in the white region, whereas no grain structure could be resolved in the darker regions (these regions are marked by white and black arrows, respectfully). The latter were assumed to be submicrometer and/or nanoscale regions, where the high density of etched grain boundaries produced darker contrasts. This was also confirmed in focused ion beam contrast images.

Figure 3 depicts the microstructural evolution for pure Fe at increasing temperatures. The annealing temperature and the percentage of the microstructure, which underwent abnormal growth, are indicated for each micrograph. Figure 4 gives a focused ion beam contrast image for nanocrystalline pure Fe annealed at 616 °C. Here, it can be seen that between the large abnormally grown grains are regions of coarse nanocrystalline grains (approximately 175 nm in diameter). Figures 5 and 6 are the same type of images; however, this time, data for the Fe 1 at.% Ni samples are shown. Again, figures 7 and 8 show the microstructure evolution for Fe 1 at.% Ta and Fe 1 at.% Zr at various temperatures and respective focused ion beam contrast images. What can be taken from images 3–8 can be summarized as follows. Changing the solute type in the following order, Fe with Ni, Ta, and Zr, increases the temperature at which abnormal grain growth occurs. Furthermore, the temperature and area fraction of existing

nanocrystalline grains increase with solute type in the same order (figure 9). Additionally, there exists a distinct difference in the stability observed between Fe with Ni and Fe with Ta or Zr, with Zr solute additions giving the highest stability.

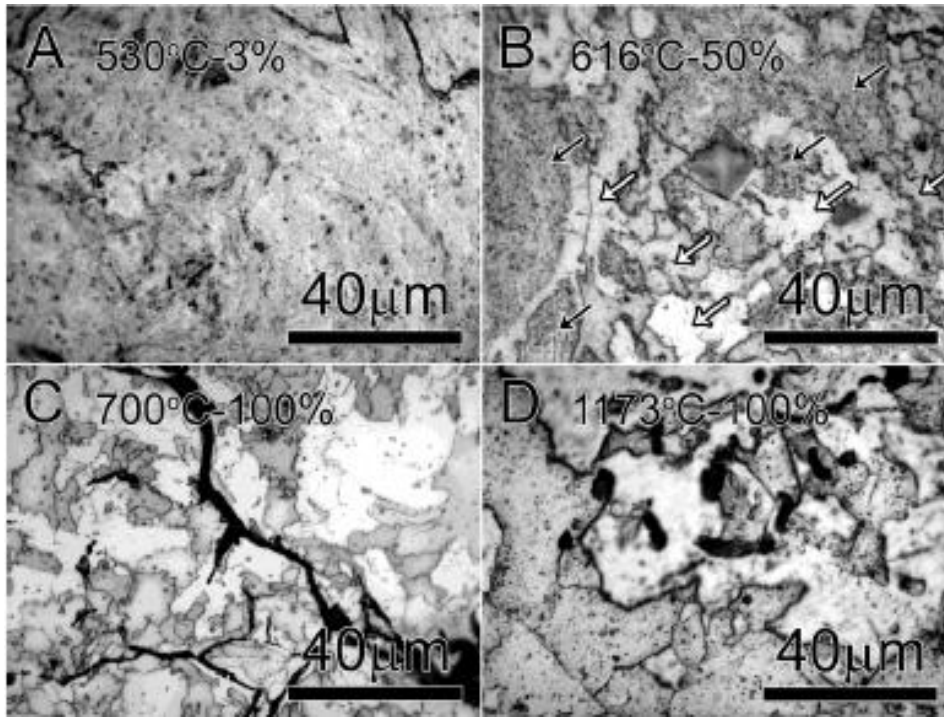


Figure 3. Optical micrographs for pure Fe after annealing 1 h at the given temperatures. Percent area abnormally grown is indicated, respectively.

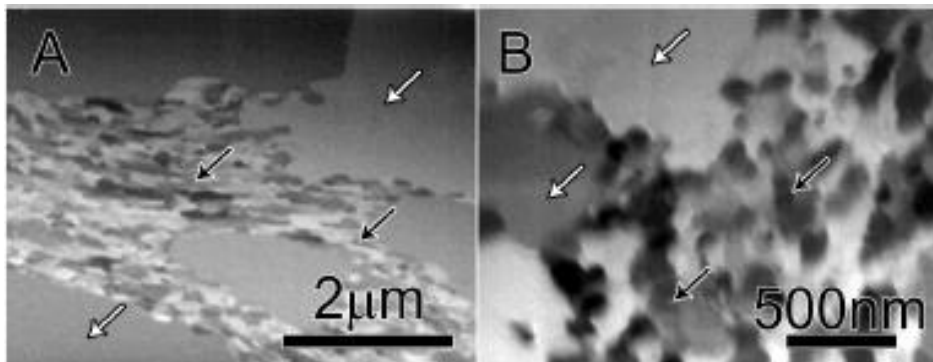


Figure 4. Focused ion beam contrast images for pure Fe after annealing at 616 °C.

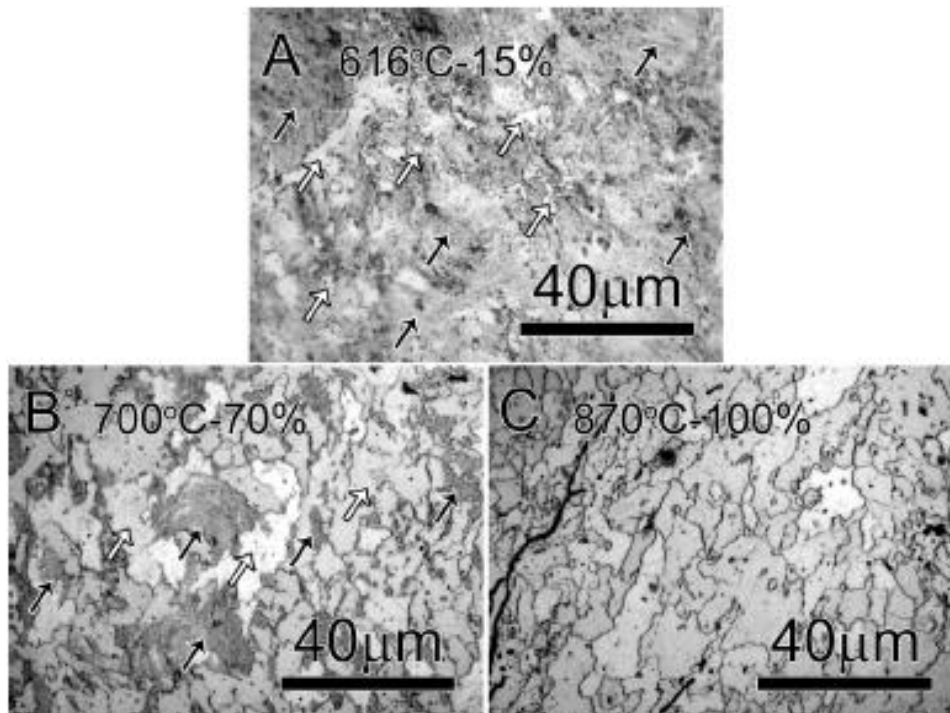


Figure 5. Optical micrographs for Fe 1 at.% Ni after annealing 1 h at the given temperatures. Percent area abnormally grown is indicated, respectively.

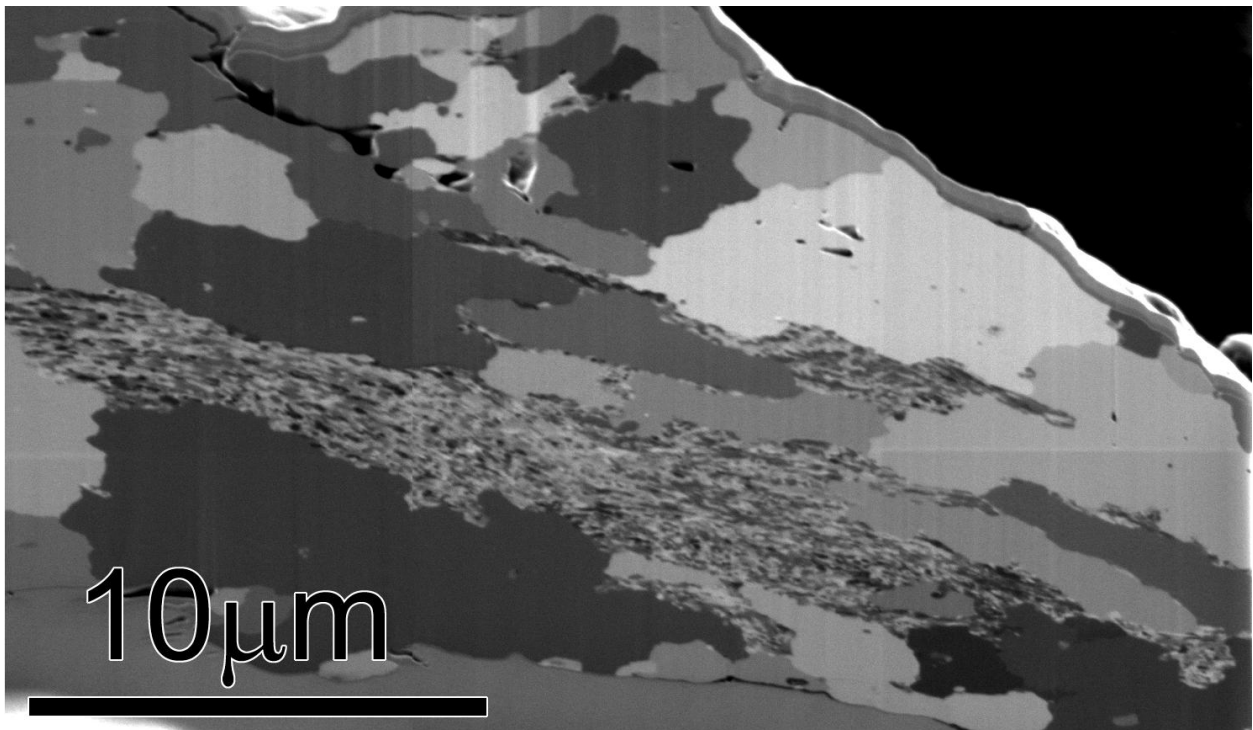


Figure 6. Focused ion beam contrast images for Fe 1 at.% Ni after annealing at 700 °C.

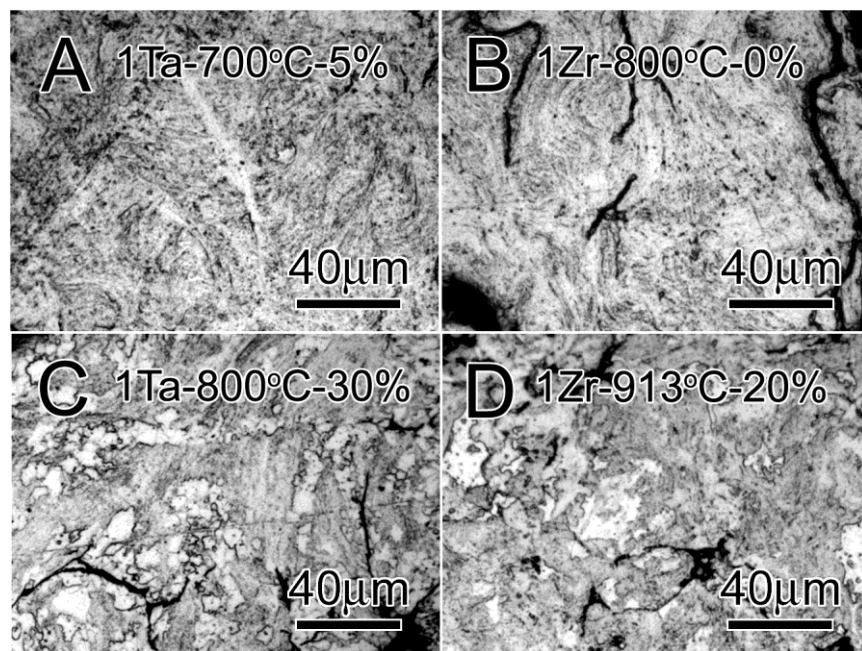


Figure 7. Optical micrographs for Fe 1 at.% Ta and Fe 1 at.% Zr after annealing 1 h at the given temperatures. Percent area abnormally grown is indicated, respectively.

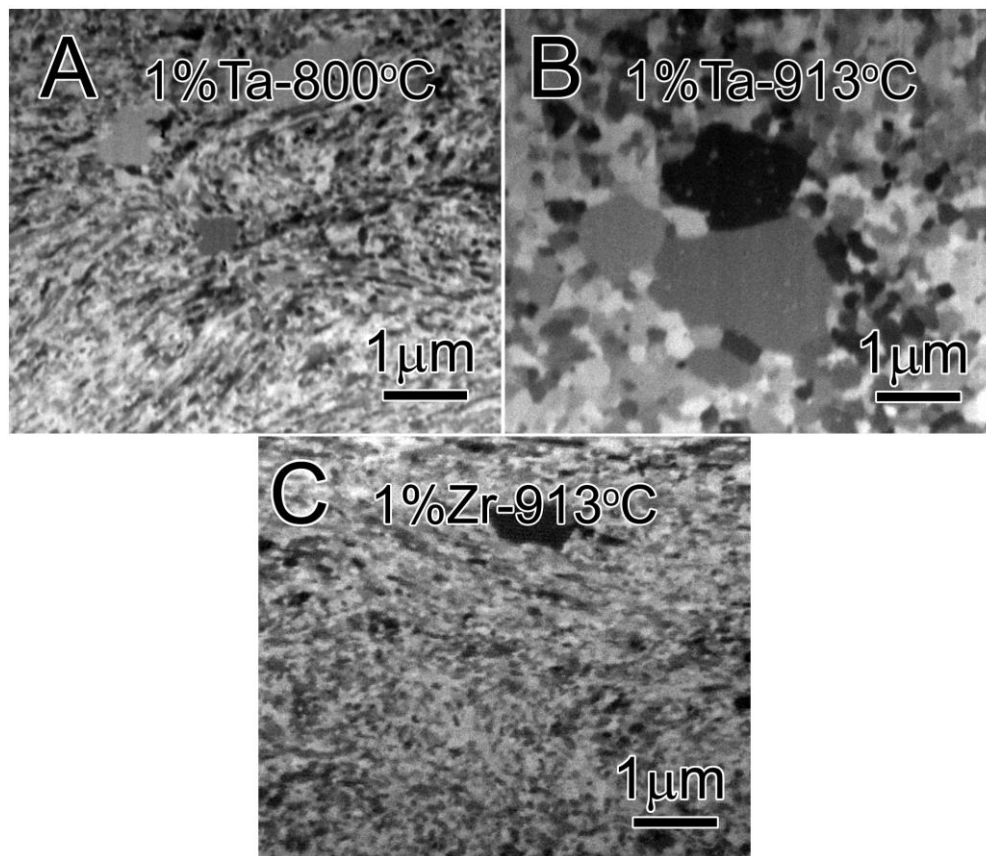


Figure 8. Focused ion beam contrast images for Fe 1 at.% Ta and Fe 1 at.% Zr after annealing 1 h at the given temperatures.

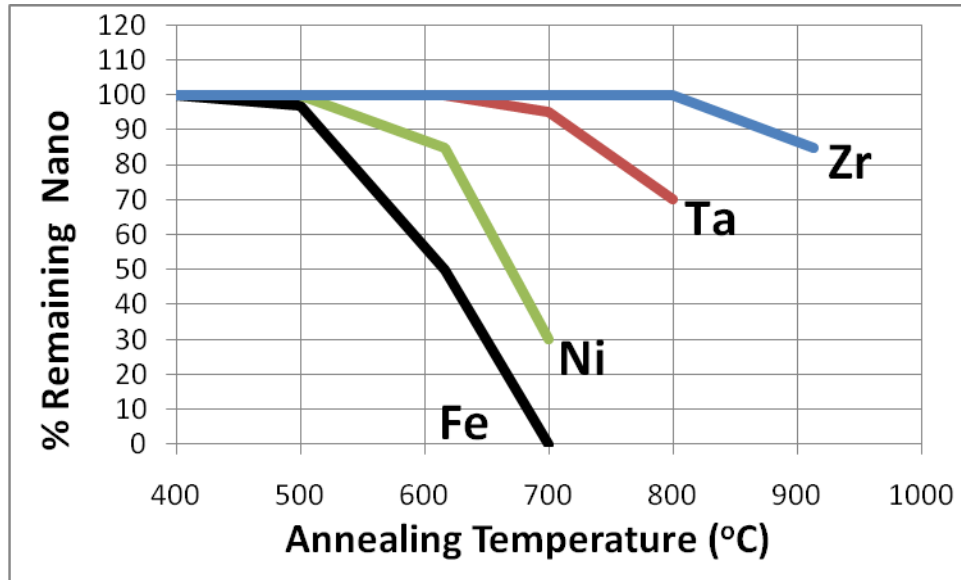


Figure 9. Plot showing the percent area remaining nanocrystalline for the various alloys vs. annealing temperature.

It can then be stated with some confidence that figure 1 predicts which solute would more effectively reduce the effective grain boundary energy in a dilute Fe alloy. Additionally, the relative depth of the free energy minima in figure 1 corresponds to the relative stability of the nanocrystalline alloys.

Due to the setbacks, the more advanced microscopy and modeling has been delayed but is currently under way. However, the initial results collected thus far are exciting. The remaining results briefly describe the preliminary aspects of this ongoing work.

Figures 10–12 summarizes current TEM findings on the Fe 1 at.% Zr system, annealed at 900 °C. Figure 10 shows low and high magnification bright field and dark field TEM images taken from a region that contained both large micrometer- and nanocrystalline-sized grains. The upper left-hand corner of each image shows the boundary between a large micrometer grain and a region containing the nanocrystalline grains. Figure 11 is a high resolution TEM image showing the location of EDS scans taken to quantify the interfacial solute concentration. Figure 12 is the solute profile for the given scanned region labeled series 1. Note that the boundary region contains a high level of Zr solute. Figures 13 and 14 give the location and solute profiles within a region of the nanocrystalline area. Also note that region GB2 shows an enrichment of Zr between the nanograins, while GB1 does not. This may indicate that solute distributions are inhomogeneous in the nanocrystalline region and could be a potential explanation for figures 15 and 16, which show the existence of regions within the microstructure which consist of high elongated grains. Additionally, inhomogeneous solute distributions within

the grain boundaries could be the potential source for abnormal grain growth. Results of ongoing compositional profiling will be used to understand how and why these phenomena are observed.

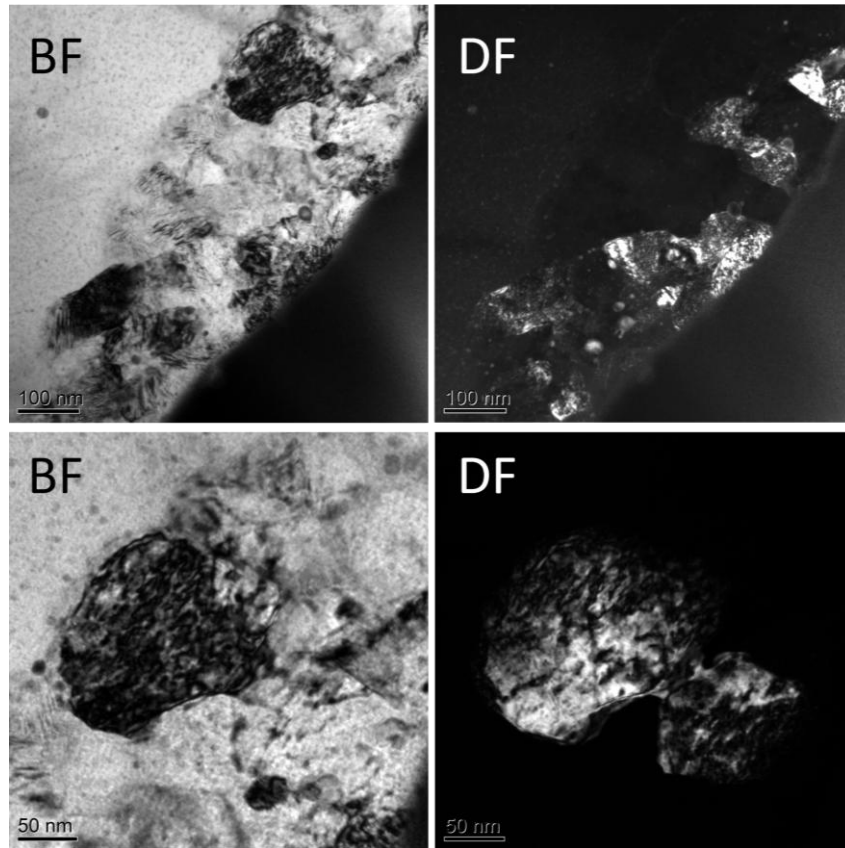


Figure 10. Bright and dark field TEM images of Fe 1 at.% Zr annealed at 900 °C. Images show a single micron-sized grain and a region containing nanocrystalline grains.

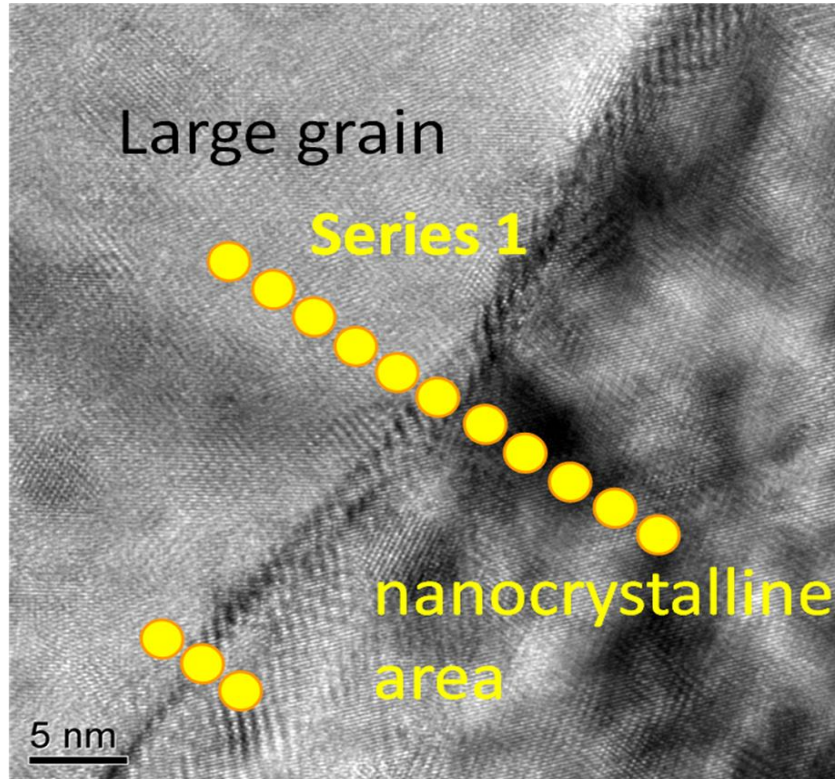


Figure 11. High resolution TEM image of Fe 1 at.% Zr annealed at 900 °C giving regions where EDS was performed to quantify Zr solute content in the boundary region.

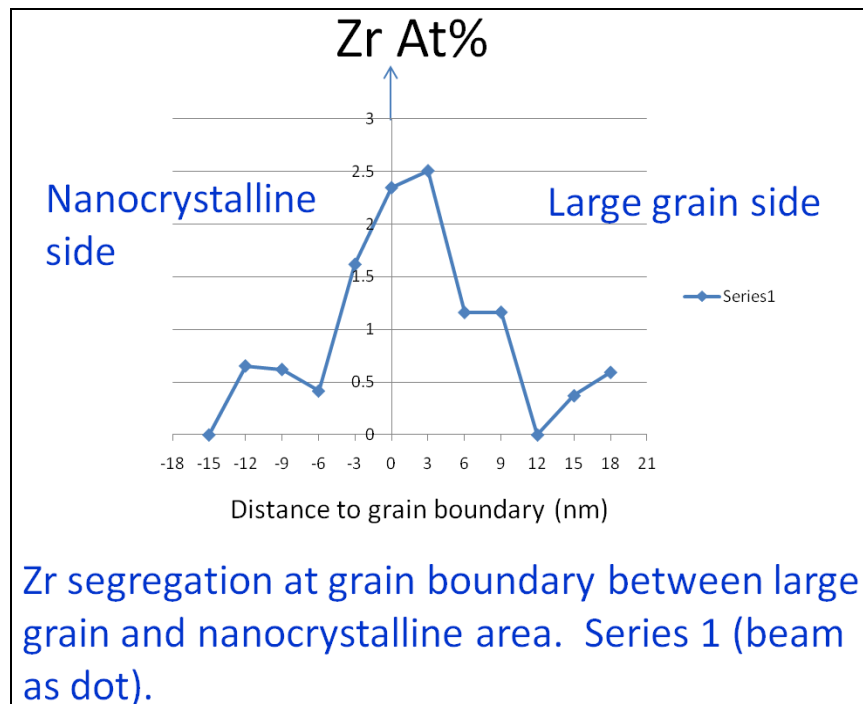


Figure 12. Corresponding solute profile for figure 11 (Series 1).

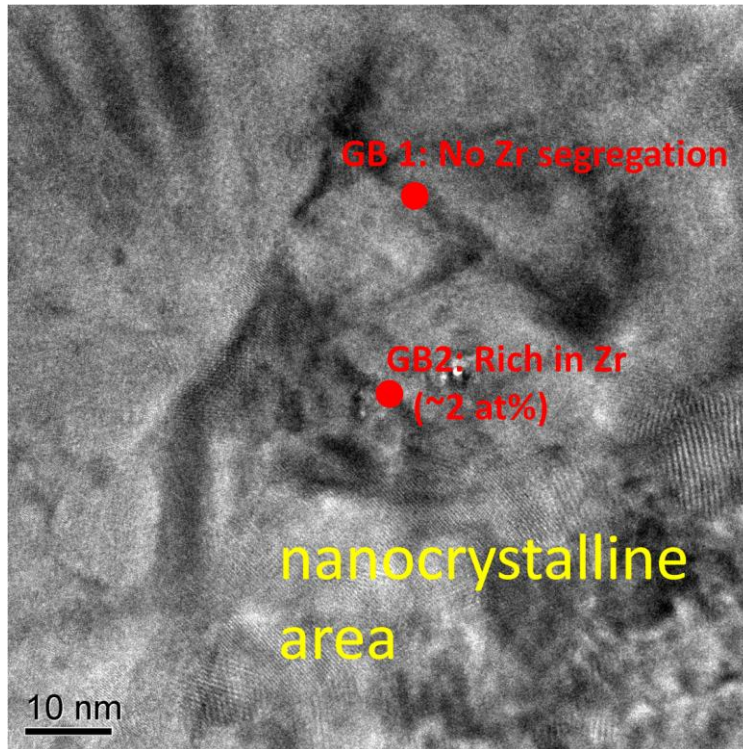


Figure 13. High resolution TEM image of Fe 1 at.% Zr annealed at 900 °C giving regions where EDS was performed to quantify Zr solute content in the boundary regions between nanograins.

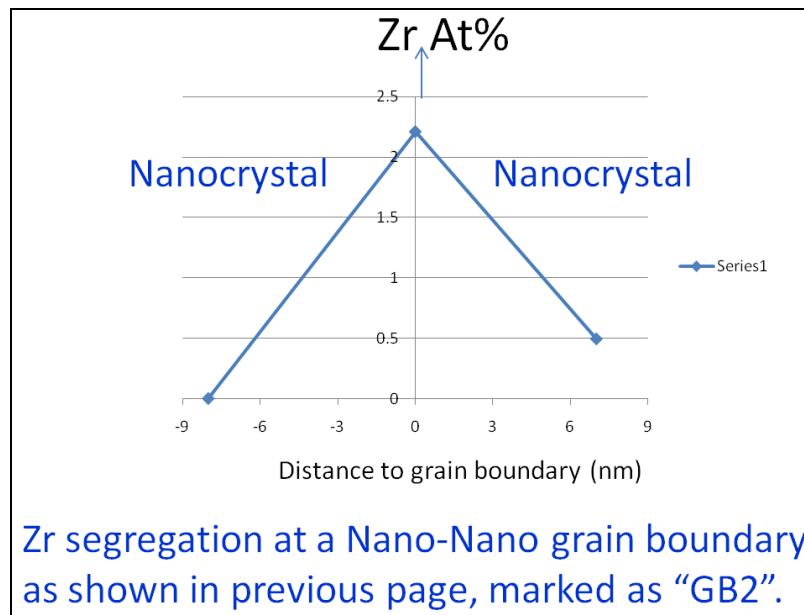


Figure 14. Corresponding solute profile for figure 13 (GB2).

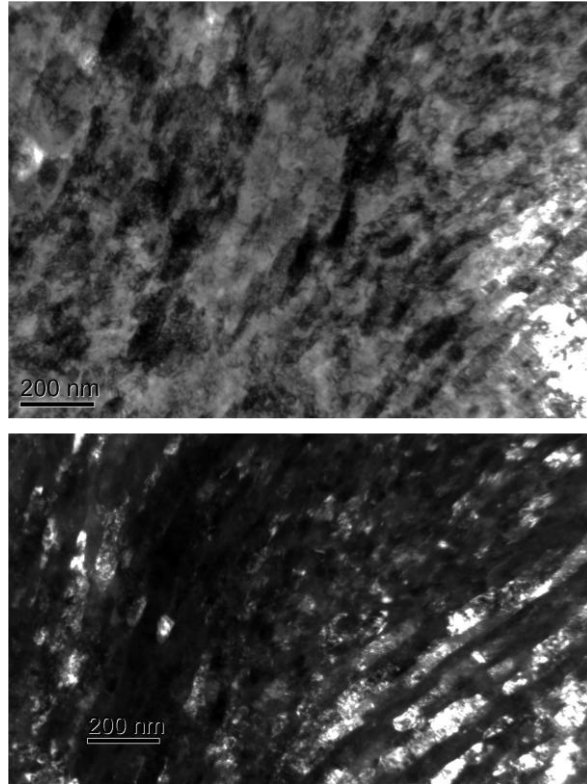


Figure 15. Bright and dark field TEM images of Fe 1 at.% Zr annealed at 700 °C. Images show elongated grain with a single micron-sized grain and a region containing nanocrystalline grains with an average aspect ratio of 10:1.

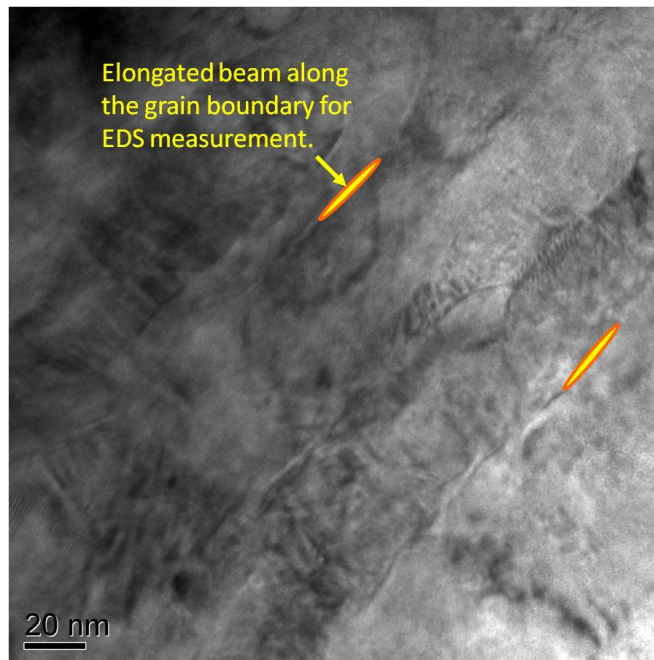


Figure 16. High resolution TEM image of Fe 1 at.% Zr annealed at 700 °C giving regions where EDS was performed to quantify Zr solute content in the boundary region.

Additional compositional profiling has uncovered a new FCC phase, which is coherent with the BCC Fe substrate matrix and has a lattice parameter of 8.5 Å (figure 17). The new phase has been observed to have two particle size distributions: particles with an average diameter of 5 nm and larger particles with a diameter greater than 20 nm. Even more intriguing is the observation that the particle with an average diameter of 5 nm appears to be pure Fe or with very low Zr content, while the larger particles are rich in Zr content (figure 18). A possible explanation is that this new FCC phase is actually the Fe₂Zr intermetallic, where the strain caused by maintaining coherency with the BCC matrix is expanding the lattice parameter from 7.1 to 8.5 Å. Additionally, it can be assumed that Fe may be occupying the sublattice sites. As the Zr concentration builds up in the lattice due to the expulsion of Zr solute from grain boundaries during grain growth, Zr can then replace the Fe to form the stoichiometric structure. Understanding how and why this phase forms may allow methods for kinetically hindering precipitation, thereby extending the temperature of stability in these systems.

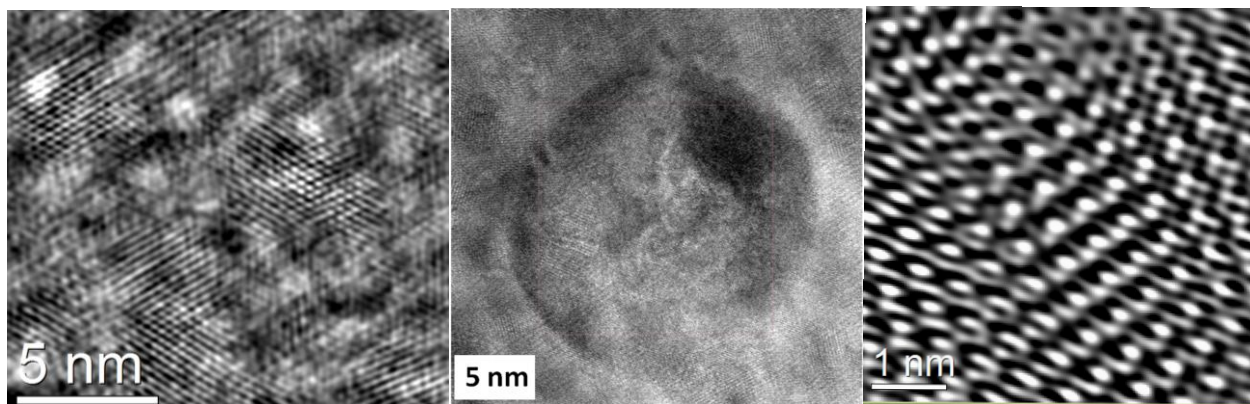


Figure 17. High resolution TEM images of Fe 1 at.% Zr annealed at 900 °C giving figure 17: Precipitates contained within abnormally grown grain. (a) Precipitates showing average size of 5 nm, (b) a larger precipitate showing coherency, and (c) a Fourier filtered high resolution TEM image using the second phase pattern in (b), showing a superlattice of FCC <110> ($a_0 = 8.5 \text{ \AA}$), which is overlapped on the α -Fe <001> lattice.

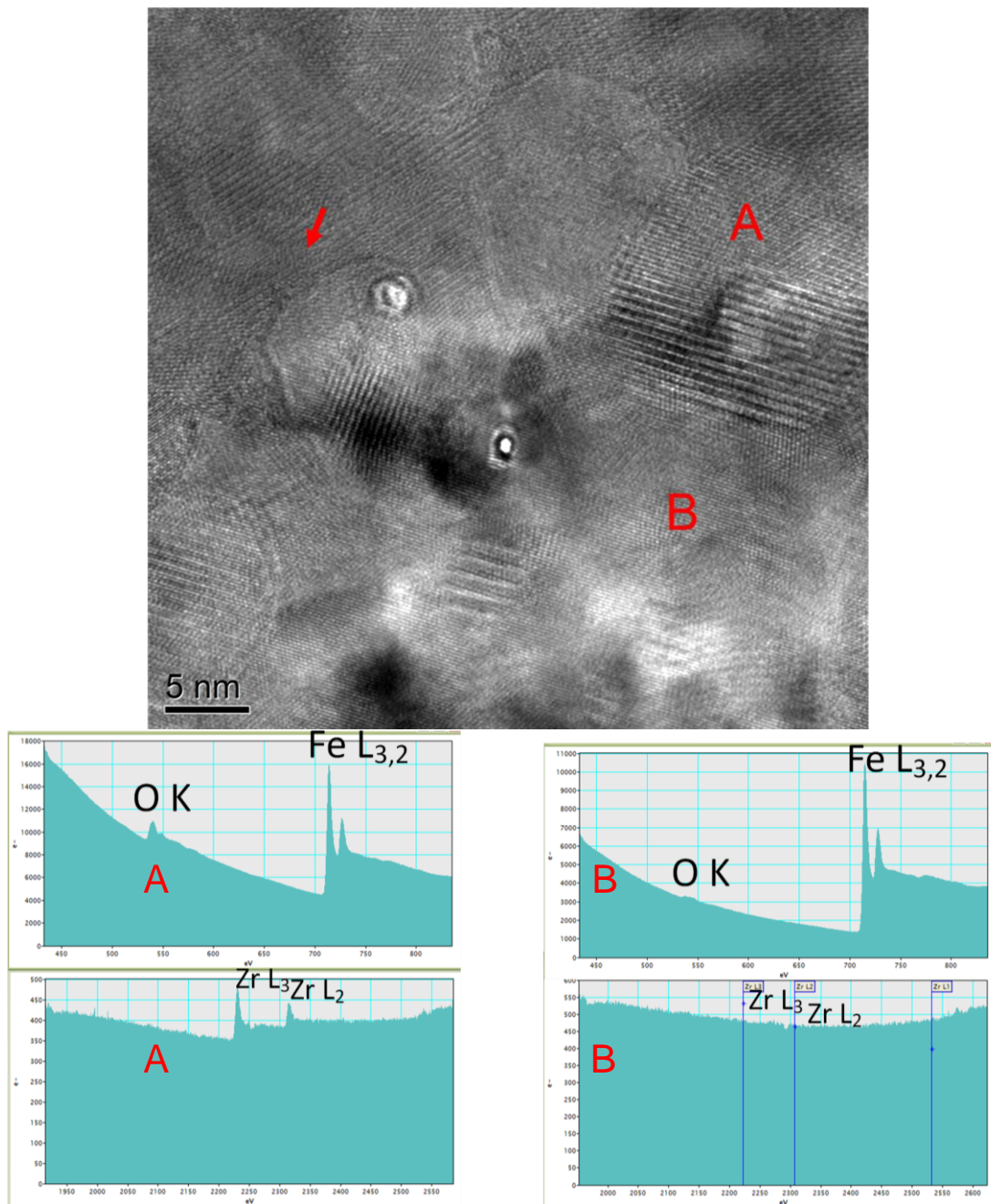


Figure 18. High resolution TEM images of Fe 1 at.% Zr annealed at 900 °C giving precipitates contained within abnormally grown grain. EELS spectra (a) and (b) for nanocrystals given in the high resolution TEM image above.

4. Conclusions

The thermal stability of nanocrystalline Fe alloys is determined by the amount of heat release associated with grain boundary segregating solutes and was correlated with experimental observations of grain growth. As suggested by the model for segregation used in this work, the addition of Ni to Fe did very little to stabilize against grain growth, while Zr had a more significant effect than Ta. In all samples, abnormal grain growth was observed to occur. The amount of abnormal grain growth increased with temperature and decreased with solute type in the following order: Ni, Ta, and Zr. The experimental observation of the increase in onset temperature for abnormal grain growth in these alloys coincided with the predicted stability. New microstructural analysis made possible by advanced microscopy techniques including high resolution imaging, EELS, and EDS analysis has lead to some interesting and important findings. Thus far, Zr solute profiles have been observed, which may yield an understanding of how grain morphology and abnormal grain growth occurs in these materials. Additionally, a new FCC phase has been identified and may hold the key on kinetically inhibiting secondary phase formation and extending thermal stability in these systems. Furthermore, current studies conducted thus far have only scratched the surface. This is such a new field and there is much to learn. It is fully expected that several ground-breaking papers will result from this work.

5. References

1. Krill, C. E.; Ehrhardt, H.; Birringer, R. *Z. Metallkd.* **2005**, *96*, 1134.
2. Abe, Y. R.; Holzer, J. C.; Johnson, W. L. *Mater. Res. Soc. Symp. Proc.* **1992**, *238*, 721.
3. Abe, Y. R.; Johnson, W. L. *Mater. Sci. Forum* **1992**, *88–90*, 513.
4. Liu, K. W.; Muchlich, F. *Acta Mater.* **2001**, *49*, 395.
5. Weissmuller, J.; Krauss, W.; Haubold, T.; Birringer, R.; Gleiter, H. *Nanostructured Mater.* **1992**, *1*, 439.
6. Terwilliger, C. D.; Chiang, Y. M. *Acta Mater.* **1995**, *43*, 319.
7. de Boer, F. R.; Boom, R.; Mattens, W.C.M.; Miedema, A. R.; Niessen, A. K. *Cohesion in Metals: Transition Metal Alloys*. Amsterdam: North-Holland, 1988.
8. Hondros, E. D.; Seah, M. P. in: R. W. Cahn, P. Haasen (Eds.), *Physical Metallurgy*, 3rd edition, Elsevier Science Pub. BV, 1983, 856–931.

6. Transitions

6.1 Journal Publications

- Stabilized Nanocrystalline Iron-based Alloys: Guiding Efforts in Alloy Selection; submitted to *Materials Science and Engineering A*.

6.2 Presentations

- A Regular Solution Model for Estimating Solute Segregation and the Stability of Nanocrystalline Fe Alloys, presented at TMS 2010, Seattle, WA, February 2010.
- Grain Size Stabilization in Nanocrystalline Fe Alloys, presented at TMS 2010, Seattle, WA, February 2010.

List of Symbols, Abbreviations, and Acronyms

Ca	calcium
Cu	copper
DFT	density functional theory
EDS	energy dispersive spectroscopy
EELS	electron energy loss spectroscopy
ELNES	energy loss near edge structure
Fe	iron
Nb	niobium
Ni	nickel
Pd	palladium
RuAl	rubidium aluminum
Ta	tantalum
TEM	transmission electron microscopy
TiO ₂	titanium oxide
Y	yttrium
Zr	zirconium

No of.
Copies Organization

1 ADMNSTR
(PDF DEFNS TECHL INFO CTR
ONLY) ATTN DTIC OCP
8725 JOHN J KINGMAN RD STE 0944
FT BELVOIR VA 22060-6218

1 HC US ARMY RSRCH LAB
ATTN RDRL CIM G T LANDFRIED
BLDG 4600
ABERDEEN PROVING GROUND MD 21005-5066

3 HCS US ARMY RSRCH LAB
ATTN IMNE ALC HRR MAIL & RECORDS MGMT
ATTN RDRL CIM L TECHL LIB
ATTN RDRL CIM P TECHL PUB
ADELPHI MD 20783-1197

11 HCS US ARMY RSRCH LAB
ATTN RDRL WMM F
K DARLING (10 COPIES)
L KECSKES
BLDG 4600
ABERDEEN PROVING GROUND MD 21005-5066

TOTAL: 16 (1 ELEC, 15 HCS)